



Supported by



Accepted Article

Title: Catalytic Activity of Ti-based MXenes for the Hydrogenation of Furfural

Authors: Michael Naguib, Wenjie Tang, Katie L. Browning, Gabriel M. Veith, Vineet Maliekkal, Matthew Neurock, and Alberto Villa

This manuscript has been accepted after peer review and appears as an Accepted Article online prior to editing, proofing, and formal publication of the final Version of Record (VoR). This work is currently citable by using the Digital Object Identifier (DOI) given below. The VoR will be published online in Early View as soon as possible and may be different to this Accepted Article as a result of editing. Readers should obtain the VoR from the journal website shown below when it is published to ensure accuracy of information. The authors are responsible for the content of this Accepted Article.

To be cited as: *ChemCatChem* 10.1002/cctc.202000977

Link to VoR: <https://doi.org/10.1002/cctc.202000977>

Catalytic Activity of Ti-based MXenes for the Hydrogenation of Furfural

Michael Naguib,^{*,[a, b]} Wenjie Tang,^[c] Katie L. Browning,^[b] Gabriel M. Veith,^[b]

Vineet Maliekkal^[c], Matthew Neurock,^{*,[c]} and Alberto Villa,^{*,[d]}

^[a] Prof. M. Naguib

Department of Physics and Engineering Physics,

Tulane University,

6823 St Charles Ave

New Orleans LA 70118 (USA)

E-mail: naguib@tulane.edu

^[b] Prof. M. Naguib, K. L. Browning, Dr. G. M. Veith

Chemical Sciences Division,

Oak Ridge National Laboratory,

1 Bethel Valley Rd.

Oak Ridge TN 37831 (USA)

^[c] Dr. W. Tang, V. Maliekkal, Prof. M Neurock

Department of Chemical Engineering and Materials Science,

University of Minnesota,

421 Washington Ave. SE,

Minneapolis MN 55455 (USA)

E-mail: mneurock@umn.edu

^[d] Prof. A. Villa

Dipartimento di Chimica,

Università degli Studi di Milano,

Via Camillo Golgi, 19

Milan MI 20133 (Italy)

E-mail: alberto.villa@unimi.it

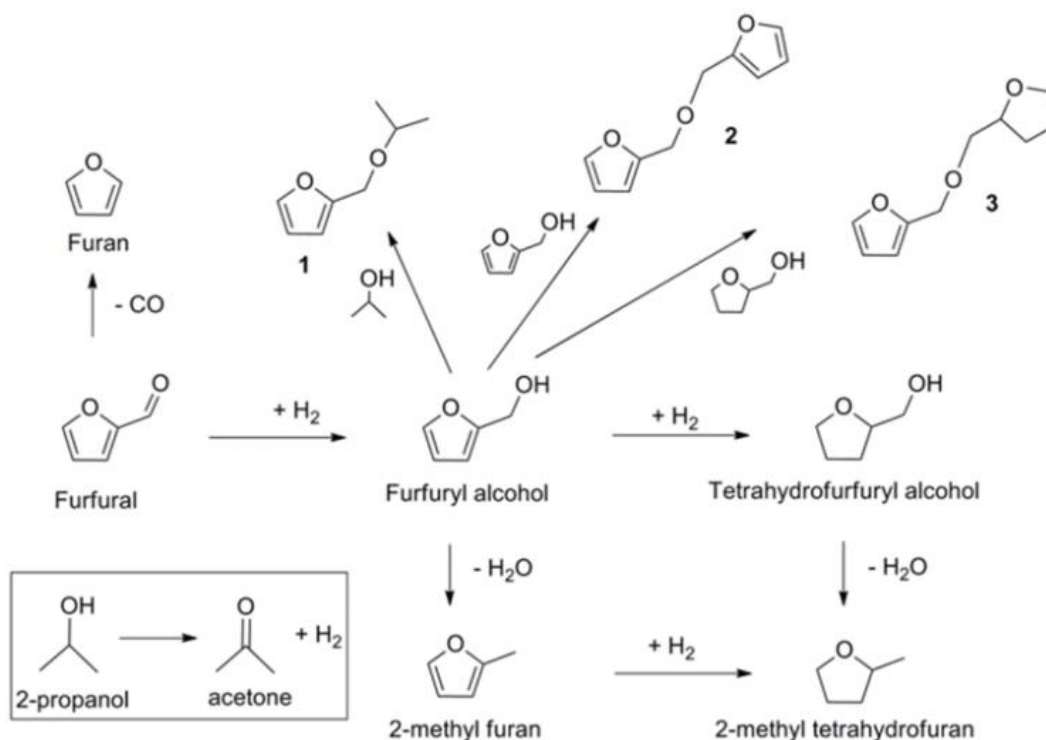
Abstract: Herein we report on the catalytic activity of Ti-based MXenes (Ti_3CNT_z and $\text{Ti}_3\text{C}_2\text{T}_z$) for biomass transformation. MXenes were found to be active catalysts for the hydrogenation of furfural using either gaseous hydrogen or 2-propanol as solvent and hydrogen source. Both catalysts showed good activity in the conversion of furfural to furfuryl alcohol, with furfuryl ether as the main by-product. Stability tests indicated that Ti_3CNT_z is more stable than $\text{Ti}_3\text{C}_2\text{T}_z$ against deactivation. Ab initio calculations were used to examine the hydrogenation and etherification reactions pathways and their corresponding reaction energetics on the Ti_3CNT_z MXene. The results indicate that the hydrogenation of the carbonyl bond efficiently proceeds via the heterolytic activation of hydrogen over the metal-oxygen site pair followed by the addition of the proton and hydride to the C and O atoms of the carbonyl. The subsequent hydrogenation of the unsaturated furan ring via metal bound hydrogen, however, is calculated to be much more difficult. Protons bound to the oxygen of the MXene are acidic and can also catalyze the etherification of the resulting alcohols. The bifunctional acid-metal site pairs also selectively catalyze the hydrogenolysis of the furfuryl alcohol to form 2-methyl furan.

1. Introduction

There has been an increasing interest in the selective transformation of lignocellulosic biomass fine chemicals and fuels over the past decade.^[1] In particular, furfural, derived from the hemicellulosic fraction of lignocellulose, is considered to be a promising platform molecule.^[1b] Indeed many of the value added chemicals such as furfuryl alcohol, an intermediate for producing resin^[3] or 2-methylfuran, a promising fuel additive for gasoline can be obtained, via selective hydrogenation and hydrodeoxygenation reaction, respectively (Scheme 1).^[4] Noble metal catalysts based on Ru, Pd and Pt^[2c, 3b, 5], and bimetallic catalysts such as PdAg^[6] have been reported to convert furfural to the above mentioned products. However, efficient catalytic materials based on non-noble-metals are preferable from an economic point of view.

Three dimensional transition metal carbides have shown a great potential as non-noble-metal catalysts for biomass conversion^[7]. In hydrodeoxygenation reaction, transition metal carbides can efficiently convert furfural to 2-methylfuran at moderate temperatures.^[8] Nanostructuring transition metal carbides increases their active surface area and enhances their catalytic activity^[9]. Carbides are well known to catalyze hydrogenation, dehydrogenation, hydrogenolysis and isomerization^[8c, 10] and have been used effectively in the hydrogenolysis of biomass.^[4, 11] Initial studies by Boudart showed that W-carbide has properties similar to Pt and can readily carry out dehydrogenation and hydrogenation reactions.^[10a] The oxygen present on many of the carbide surfaces is strongly bound and in the presence of hydrogen can readily form Brønsted acid sites that can carry out acid catalyzed reactions and can promote along with metal sites hydrogenolysis. Bhan^[7b], for example, showed the presence of both metal and acid sites on Mo₂C and demonstrated how these sites and their reactivity can be tuned by the selective addition of oxygen.

Recently, a new family of two-dimensional (2D) transition metal carbides and carbonitrides, so-called MXenes, has been developed by the selective etching of atomically thin metal layers from layered ternary carbides and carbonitrides called MAX phases.^[12] MXenes have a general composition of M_{n+1}X_nT_z where M stands for an early transition metal (Ti, V, Cr, Nb, Mo, etc.), X stands for carbon and/or nitrogen, T_z stands for a mixture of the surface terminations (O, OH, F) that resulted from the etching in F-contained aqueous solution, and n =1-3. With more than 15 unique members synthesized so far (e.g. Ti₃C₂T_z, Nb₂CT_z, TiNbT_z, Mo₂CT_z), MXenes are the fastest growing family of 2D material. Similar to transition metal carbides, MXenes are electrically conductive.^[12c, 13]



Scheme 1 Proposed pathways for furfural hydrogenation.

These materials are similar to the carbides and may offer significant promise in terms of controlled functionalization and tunability. Thanks to their surface terminations, MXenes are hydrophilic.^[12c] This combination of hydrophilicity and electronic conductivity is very rare in 2D materials. MXenes also exhibit a highly negative zeta potential in neutral and high pH values which allows them to disperse easily in water.^[14] MXenes were found to be promising for many applications such as electrochemical energy storage,^[15] water purification^[16] and sensing^[17].

In the catalysis area, MXenes have been explored as supports for catalytic materials like Pt,^[18] Ru,^[19] RuCo,^[20] RuNi,^[21] and CuO₂.^[22] MXenes were also found to help promote or co-catalyze some reactions.^[23] For example, adding 5 wt% of Ti₃C₂T_z to rutile resulted in 4 times enhancement in visible-light photocatalytic hydrogen evolution compared to pure rutile.^[23b] Liu et al. reported on a significant reduction in the dehydrogenation onset temperature of MgH₂ (reduced from 278 °C to 185 °C) by adding 5 wt.% of Ti₃C₂T_z.^[24] Combining carbon nitride nanosheets with Ti₃C₂T_z resulted in a high electrocatalytic activity when tested for oxygen-evolution reaction.^[25] MXenes were also found to be promising electrocatalyst for hydrogen evolution reaction.^[25-26] Moreover, it has been demonstrated that TiO₂ are active in the transfer hydrogenation of C=O bond.^[27] Diao *et al.*, reported that Ti₃C₂T_z can catalyze ethylbenzene dehydrogenation with a reactivity of 92 μmol m⁻² h⁻¹.^[28] Recently,

Blanco *et al.* showed that can be used for hydrodeoxygenation (HDO) of guaiacol resulting in phenol and methylanisole^[29]. Interestingly, they showed that the MXene surface has both weak acid and basic sites.

In the present work we report for the first time on the catalytic activity of MXenes in the selective hydrogenation of furfural, a molecule derived from hemicelluloses.^[4] In particular we show that Ti-MXenes (*viz.* $\text{Ti}_3\text{C}_2\text{T}_z$ and Ti_3CNT_z) promote the hydrogenation to furfuryl alcohol, ethers and the hydrodeoxygenation to 2-methyl furan. $\text{Ti}_3\text{C}_2\text{T}_z$ and Ti_3CNT_z were selected for this study since the former was the first reported MXene^[12b] and the most studied MXene. The latter is the only carbonitride MXene reported so far, which would allow us to study the role of nitrogen in the catalytic reaction for the same transition metal MXene.

2. Results and Discussion

Ti MAX phases and their corresponding MXenes were prepared following the procedure reported by Naguib *et al.*^[12a, 12b] Synthesis of both $\text{Ti}_3\text{C}_2\text{T}_z$ and Ti_3CNT_z was confirmed by using X-ray diffraction. As shown in Figure 1, etching Al from MAX phases resulted in vanishing the 100% peaks (around 2θ of 39°) and broadening of the (0002) peaks.

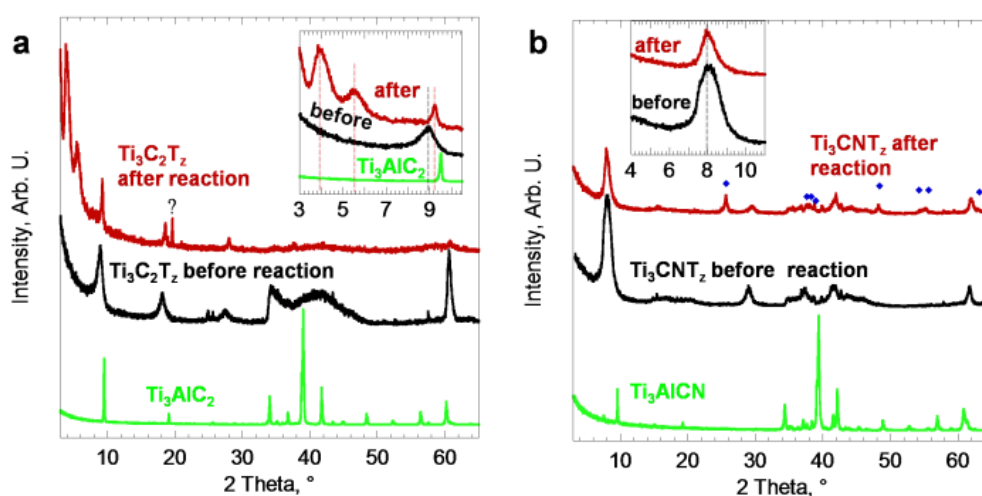


Figure 1. X-ray diffraction patterns of samples before and after reaction for a) $\text{Ti}_3\text{C}_2\text{T}_z$ and b) Ti_3CNT_z , detailed (0002) peak areas are presented in the insets. The blue diamonds in the Figure b represent the peaks position of Anatase [PDF#02-0406].

The catalysts were tested for the hydrogenation of furfural under hydrogen or using 2-propanol as hydrogen source (453 K, 5 bar H_2 or N_2). The results are presented in Table 1 and Table S1 and Figure 2.

Table 1. Furfural hydrogenation in 2 propanol. ^[a]

Catalyst	Pressure (bar), gas	Activity ^[b] (%)	Conv (%)	Selectivity (%) ^[c]				Mass Balance (%)
				Furfuryl alcohol	2-methyl-furan	Ethers		
						1	2	
No-cat	5, N ₂	-	2	-	-	-	-	-
Ti ₃ CNT _z	5, N ₂	72	46	49	17	23	9	98
Ti ₃ C ₂ T _z	5, N ₂	88	36	52	10	23	11	97
No-cat	5, H ₂	-	3	-	-	-	-	-
Ti ₃ CNT _z	5, H ₂	126	59	43	25	23	5	96
Ti ₃ C ₂ T _z	5, H ₂	145	62	49	13	27	6	95

[a] Reaction conditions: Furfural = 0.3 M; F/catalyst ratio = 50 wt/wt, 453 K, 5 bar N₂, reaction time 48 h. [b] Activity (Converted mmol_{furfural} g_{catalyst}⁻¹ h⁻¹), calculated after 3 h of reaction. [c] Selectivity at 35% of conversion.

Both catalysts showed higher activity when H₂ was used instead of N₂, but the selectivity is not significantly influenced by the hydrogen source (Table 1). Ti₃C₂T_z showed a higher initial (after 3 h) activity (88 and 145 converted mmol_{furfural} g_{catalyst}⁻¹ h⁻¹, using N₂ and H₂ respectively) compared to Ti₃CNT_z (72 and 126 converted mmol_{furfural} g_{catalyst}⁻¹ h⁻¹, using N₂ and H₂ respectively). However, comparing the conversion after 48 h, Ti₃CNT_z is more active than Ti₃C₂T_z (46% and 36% conversion for Ti₃CNT_z and Ti₃C₂T_z at bar 5 N₂, respectively, Table 1). On the contrary, in presence of H₂ a similar conversion over the Ti₃CNT_z and Ti₃C₂T_z was achieved (59% and 62% conversion for Ti₃CNT_z and Ti₃C₂T_z, % bar H₂).

Indeed, by examining the reaction profiles (Figure 2a), it can be observed that Ti₃C₂T_z underwent evident deactivation when N₂ was used. The resistance against deactivation was investigated performing stability tests in presence of N₂ (Figure 2b). Recycling experiments were carried out by filtering and using the catalyst in the next run without any further purification. Ti₃CNT_z exhibits good stability for six consecutive runs, whereas Ti₃C₂T_z confirmed the lower resistance to deactivation.

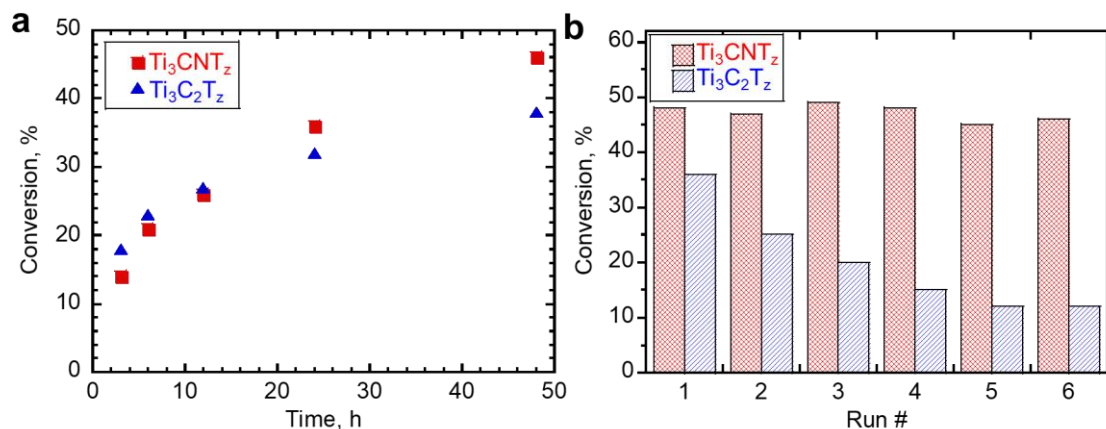


Figure 2 Catalytic performance of $Ti_3C_2T_z$ and Ti_3CNT_z a) reaction profiles, and b) stability test.

The selectivity of $Ti_3C_2T_z$ and Ti_3CNT_z were compared at iso-conversion (35%) showing a similar trend, regardless of the utilization of H_2 or N_2 . Furfuryl alcohol was the main product for $Ti_3C_2T_z$ and Ti_3CNT_z , respectively (Table 1), indicating a very similar active site. 2-methylfuran and ethers were also obtained as by-product (Table 1). Ti-based MXenes also showed the ability to promote the hydrodeoxygenation reaction to 2-methyl furan. Ethers, deriving from the etherification of furfural with the solvent (2- propanol) or furfuryl alcohol were also found (Table 1). Only traces of tetrahydrofurfuryl alcohol (THFA) were obtained, evidence that Ti-based MXenes are not able to hydrogenate the furanic ring under these reaction conditions. By analyzing the selectivity at different reaction times (Table S1), we observed a decreased selectivity to furfuryl alcohol with the formation of higher amount to 2-methylfuran and increasing the conversion. The result confirmed that methyl furan is derived from the successive hydrogenolysis of furfuryl alcohol (Scheme 1).

XRD, SEM and XPS investigation of the catalysts after reaction were performed and compared to the fresh ones, to address the different stability during the reaction of the two catalysts (Figure 1,3 and 4). Figure 1 shows the XRD patterns for both $Ti_3C_2T_z$ and Ti_3CNT_z before and after testing. In both cases, MXene peaks were preserved but with changes in *c* lattice parameter (LP). As shown in the inset of Figure 1a, the 0002 peak of pristine $Ti_3C_2T_z$ at 2θ of 8.96° (*c*-LP 19.7 Å) was replaced by 3 peaks after testing. One of the peaks was located at higher angle (2θ of 9.24°) that corresponds to *c*-LP of ~ 19.1 Å. The other two peaks were shifted to lower angles of 3.94° and 5.56° (corresponding to *c*-LP 44.8 and 31.8 Å, respectively) compared to pristine MXene. Assuming that they all have similar chemical composition, by comparing the area under the three new 0002 peaks it reasonable to suggest that the $Ti_3C_2T_z$ with *c*-LP 44.8 is the major MXene (areas of 0002 peaks for *c*-LP 44.8 : 31.8 : 19.1 Å ~ 3.5 :

1.0 : 1.0) after testing. The increase in the MXene lattice parameter can be explained by intercalating some of the catalytic reaction by-products that trapped between the layers and pillared the structure. Similar phenomena were reported upon cycling MXenes in Li,^[30] Na,^[31] and K ion batteries^[15i]. The presence multiple intercalations states after the reaction (evidenced by the 3 different 0002 peaks instead of only before the reaction) is most likely due to presence of various surface terminations on the MXenes surface that interact differently with the reactants. This suggests that there is a large room for tuning the MXenes surface chemistry to target certain reaction. A new sharp peak at 2θ of 19.61° appeared after the reaction but it could not be identified. Unlike $\text{Ti}_3\text{C}_2\text{T}_z$, Ti_3CNT_z showed no change in the *c*-LP ($\sim 21.9 \text{ \AA}$) after the reaction, but new peaks corresponding to anatase emerged after the reaction. Nitrogen contained MXenes are predicted to be less stable than their carbides counterparts,^[32] which may explain the presence of anatase in case of Ti_3CNT_z and its absence in case of $\text{Ti}_3\text{C}_2\text{T}_z$ after being exposed to the same testing conditions. Nitrogen in carbonitride MXene render the layers to be much more highly negatively charged (with zeta potential of -65 mV around neutral pH) compared to their carbide counterpart,^[14] that lead to spontaneous intercalation of aluminum ions from the etching process of the parent MAX phase during the synthesis resulting in a larger *c*-LP of Ti_3CNT_z compared to $\text{Ti}_3\text{C}_2\text{T}_z$ ^[33]. The presence of a single Ti_3CNT_z 0002 peak after the reaction compared to the three of $\text{Ti}_3\text{C}_2\text{T}_z$ can be explained by the less diverse surface termination. For example, our recent neutron scattering study showed that Ti_3CNT_z has significantly lower content OH terminations compared to $\text{Ti}_3\text{C}_2\text{T}_z$ ^[33].

By comparing the SEM images of MXenes before (Fig. 3a and 3c for $\text{Ti}_3\text{C}_2\text{T}_z$ and Ti_3CNT_z respectively) and after the reaction (Fig. 3b and 3d for $\text{Ti}_3\text{C}_2\text{T}_z$ and Ti_3CNT_z respectively), it is clear that nano-features appeared on the MXenes surfaces and in-between the layers after the reaction. For $\text{Ti}_3\text{C}_2\text{T}_z$ the layers were fully covered with small uniform nano-features. In case of Ti_3CNT_z , these features were larger, and the particles surfaces were more charging which agrees with the presence of anatase detected by XRD.

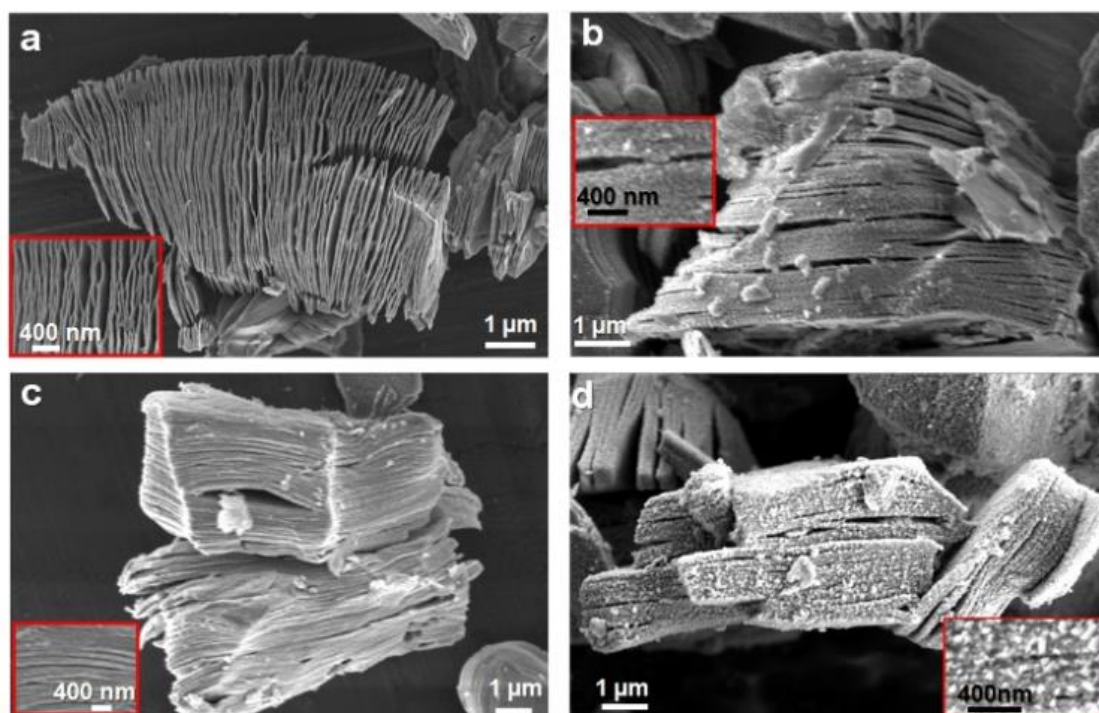


Figure 3 SEM images of $\text{Ti}_3\text{C}_2\text{T}_z$ a) before and b) after the reaction, and Ti_3CNT_z c) before and d) after the reaction. The insets are higher magnifications for the surfaces.

Moreover, XPS of $\text{Ti}_3\text{C}_2\text{T}_z$ revealed a weaker Ti 2p signal compared to the pristine surface (Figure 4a), evidencing a lower amount of Ti groups on the surface after the reaction. This phenomenon can be ascribed to the irreversible adsorption of reactants and reaction products on the surface as suggested by SEM and XRD analyses. Partial leaching of Ti into the solution (1%, measured by atomic absorption spectrometry, AAS) may contribute to the weaker Ti 2p signal (Figure 4a). Oxidation of Ti cannot be excluded as one of the deactivation mechanisms of $\text{Ti}_3\text{C}_2\text{T}_z$. These phenomena can be responsible of the evident deactivation of $\text{Ti}_3\text{C}_2\text{T}_z$ (Figure 2). On the contrary, the more stable behavior of Ti_3CNT_z can be justified by the absence of any changes in the *c*-LP after the reaction (Figure 1b). As shown in Figure 4b, Ti 2p XPS peak for Ti_3CNT_z after the reaction was found to be strong which suggests that Ti sites were not covered by reaction products. Moreover, no leaching occurred as confirmed by AAS. Though there is a loss of low energy Ti 2p and C 1s species (456 and 282 eV) indicate that carbides on the initial surface are reacted away in solution resulting in Ti^{4+} surface termination.

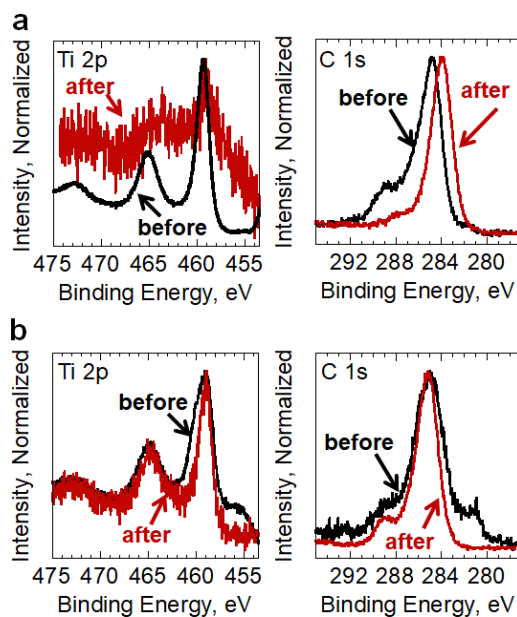


Figure 4. XPS core levels of Ti 2p and C 1s for a) $\text{Ti}_3\text{C}_2\text{T}_z$ and b) Ti_3CNT_z before and after the reaction.

It is worth noting that when different TiO_2 materials (rutile, anatase and P25) were tested under the same conditions as MXenes, they showed very low activity (Table 2). The activity of the prepared Ti MXenes was compared to the activity of metal carbides and noble metal free catalysts reported in the literature, showing comparable or even better activity (Table 2).

Table 2. Comparison of the activity different Ti based catalysts and metal carbides for furfural (FA) hydrogenation

Catalyst	T (K)	Pressure (bar), gas	FA/catalyst ratio wt/wt	Activity ^[a]	Selectivity (%)		Ref
					Furfuryl alcohol	2-methyl-furan	
Ti ₃ CNT _z	453	5, N ₂	50	72	49	17	This work
Ti ₃ C ₂ T _z	453	5, N ₂	50	88	52	10	This work
TiO ₂ P25	453	5, N ₂	50	7	40	-	This work
TiO ₂ Rutile	453	5, N ₂	50	8	45	-	This work
TiO ₂ anatase	453	5, N ₂	50	3	30	-	This work
TiO ₂	423	1, N ₂	3.2	10	57	-	[27a]
NiO	423	1, N ₂	3.2	18	97	-	[27a]
Ni0.5MoC–SiO ₂	423	60, H ₂	3	7	70	25	[34]
MoC	423	3, H ₂	6.6	15	10	89	[35]
Ni/SiO ₂	353	34, H ₂	10	2	49	-	[36]
Co/SiO ₂	353	34, H ₂	10	2	53	-	[36]
Cu/MgO–Al ₂ O ₃	493	1, N ₂	4	42	90	-	[37]
NiFe ₂ O ₄	493	n.d.	3	0.3	71	-	[38]
Fe ₂ O ₃ @HAP	493	10	2.4	1.0	92	-	[39]

[a] Activity (Converted mmol_{furfural} g_{catalyst}⁻¹ h⁻¹)

First principle density functional theory (DFT) calculations were carried out to help elucidate the reaction pathways, mechanisms and the nature of the active sites that control the hydrogenation of furfural. The calculations predominantly examined the use of H₂ as a hydrogen source. The synthesized MXene structures are thought to be covered with oxygen or hydroxyl species (Figure 5c). Under the strongly reducing condition used to carry out catalysis, however, the surface OH species can be removed as water with a barrier of 1.05 eV (Figure S1). As such, the MXene surface is thought to be covered with O*, OH* and H* species under reducing conditions. This is consistent with the presence of metal and acid (OH) sites on metal carbide surfaces under reaction conditions^[4]. The elementary adsorption, surface reaction and desorption steps involved in the selective hydrogenation, hydrogenolysis and etherification paths shown in Scheme 1 were calculated on the MXene surface covered in OH* and O*. The detailed reactant, transition and product state structures for the reactions

considered are shown in Figures S1-S3. At the high coverages of OH*, O* and H* found under operating conditions, the rate is ultimately controlled by the elementary step with the highest intrinsic activation barrier where the adsorption and desorption steps are quasi-equilibrated. We therefore highlight the highest intrinsic barrier steps in the potential energy cycles for the hydrogenation and hydrogenolysis reactions reported in Figures S5-S6 and the etherification reactions reported in Figures S7. We simplify these energy cycles in the in Schemes 2-3 which report the highest intrinsic barriers for the particular hydrogenation, hydrogenolysis and etherification paths. We discuss each of the different paths below.

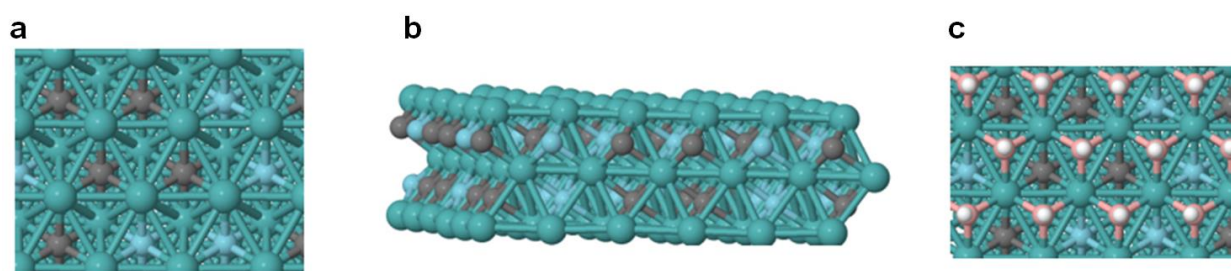


Figure 5. a) Top view and b) side view of a monolayer of Ti_3CN MXene in the absence of OH termination; c) top view of MXene surface covered with OH species. The Ti, C, N, O, H atoms are represented by green, black, cyan, pink and white, respectively.

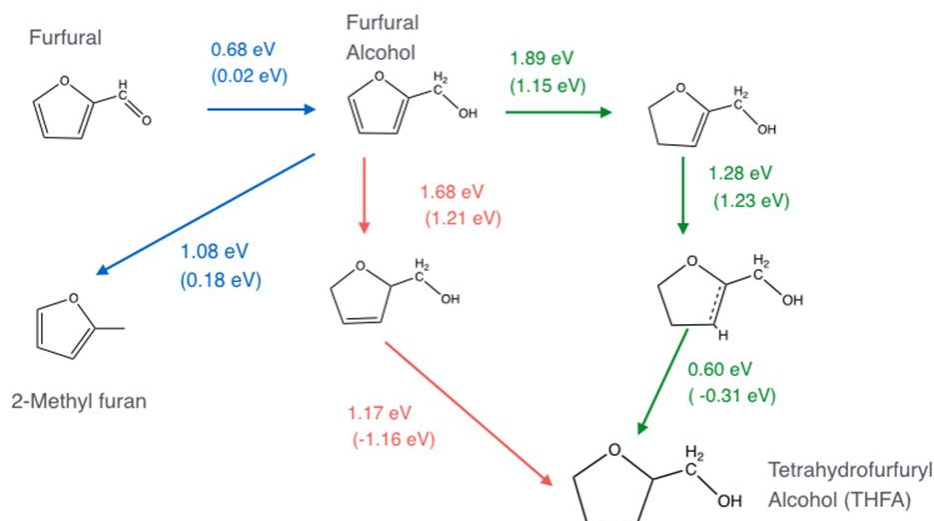
Vacancy sites were formed via the reaction between two OH* groups to eliminate water. Hydrogen is readily activated over metal-metal site pairs to form two M-H bonds with a very small barrier of 0.08 eV or over metal-oxygen site pairs to form M-H and O-H bonds with a barrier of 0.48 eV as shown in Figure S2. A charge analysis for the dissociation of hydrogen over the M-O bond shows that H_2 splits heterolytically resulting in a charge of +0.65e for the proton bound to the oxygen and a charge of -0.55e for the hydride bound to the metal. This proton and hydride combination is of importance for the subsequent hydrogenation of furfural discussed later.

Furfural binds to the TiO-H Brønsted acid sites on the MXene surface with an adsorption energy of -0.54 eV. This is similar to the adsorption of aldehydes and ketones to an acid site in zeolites and other heterogeneous acid catalysts. The C=O bond is subsequently hydrogenated via the addition of the surface hydride to the carbonyl carbon. The proton transfer step occurs very rapidly and without a barrier upon the addition of the hydride (see Figure S5). For simplicity, we therefore consider this as a single coupled hydride-proton transfer step with a barrier of 0.68 eV to form the resulting furfuryl alcohol (FA), as shown in Scheme 2 and Figures S3a. In the transition state shown in Figure S8, the hydride that transfers from the metal is stabilized by its interaction with two metal sites and the carbon to which it

ultimately binds. The charge on the proton in the transition state is $+0.69e$ whereas the charge on the O is $-0.63e$.

For comparison, we also examine the transfer hydrogenation of furfural using 2-propanol. The reaction is somewhat similar to that found using H_2 in that the proton from the alcohol readily transfers with a barrier to the bound furfural. The rate is dictated by the hydride transfer from the bound 2-propoxy. The transition state for this reaction is shown in Figure S9. The barrier for this step is 1.01 eV which is a somewhat higher than the 0.68 eV barrier for hydrogenation using H_2 . This is consistent with the experimental results which show higher activities when H_2 was used as the hydrogen source over 2-propanol.

The subsequent hydrogenation of the C=C bond of FA to form 3,4 dihydrofurfuryl alcohol, 4,5 dihydrofurfuryl alcohol and the fully saturated tetrahydrofurfuryl alcohol, which are shown in detail in Figures S3c-g and S6 and summarized in Scheme 2, have activation barriers of 1.68 eV, 1.89 eV and 1.2 eV, respectively. These barriers are 2-3 times higher than that for the hydrogenation of FA thus indicating that the formation of THFA is unlikely. The high barriers for forming THFA agree very well with the fact that only traces of THFA were found in the experiment.



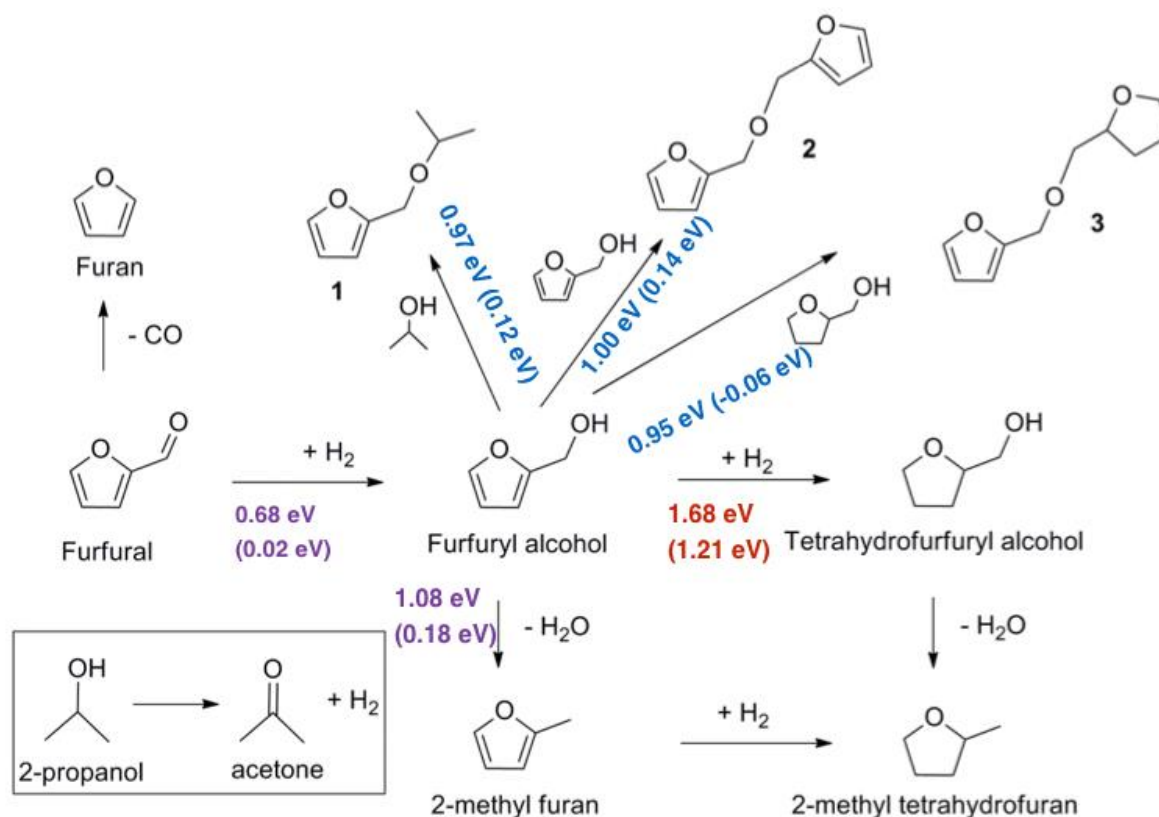
Scheme 2. Furfural hydrogenation scheme. The details of atomic structures are shown in Figure S3.

As shown in Figure S6c (see structures in Figure S3b) and Scheme 2, 2-methyl furan is another major product that is formed via hydrogenolysis. This reaction selectively proceeds via the coupling of metal and acid site pairs that aid in the addition of hydrogen and removal of water via dehydration, respectively. Similar to the hydrogenation of the carbonyl of furfural, hydrogen heterolytically dissociates to form a proton and a hydride that then add to the C-O

bond of FA and eliminate water to form 2-methyl furan. The step has a barrier of 1.08 eV that is readily accessible at the reaction temperature 453 K. Alcohol dehydration over supported heteropolyacid catalysts with similar barriers of 1.1 eV show experimental rates of dehydration of $0.001 [\text{s H}^+]^{-1}$ at 343 K^[40] The rates for such systems at 453 K would be as high as $20 [\text{s H}^+]^{-1}$. The reaction proceeds via the simultaneous addition of a surface proton to OH group of FA, the elimination of H₂O and a hydride addition to the methylene group of FA.

Beside 2-methyl furan, ethers are likely to form by the coupling of two alcohols. Based on different alcohols present under experimental conditions, 3 different ethers can be generated, as shown in Scheme 3 and Figure S7 (structures reported in Figure S4). All of the ethers form via the same Brønsted acid catalyzed mechanism where a surface proton attacks the OH group of the first alcohol to eliminate water. The proton on the second alcohol is then abstracted by surface O site. The resulting alkoxide then attacks the alpha-C of the first alcohol to form the C-O bond thus generating the ether. The activation barriers to form difurfuryl ether, furfuryl-2propyl ether, and furfuryl-tetrahydrofurfuryl ether formation are all similar falling in the range from 0.95 to 1.00 eV. These ether formation barriers are all significantly lower than the barriers for THFA formation, which explains the higher selectivity toward the ether products found in experiment.

The calculated results show that the proton coupled hydride addition to be especially efficient for hydrogenation of polarized bond such as C-O bond. The C-C bonds of the furan ring, on the other hand, are difficult to hydrogenate. The surface OH species act as acid that readily catalyze ether formation. The presence of the metal and acid site pairs on the MXene surface also drive the selective hydrogenolysis of the C-OH bond of furfuryl alcohol. This is consistent with presence of bifunctional sites that drive the hydrogenolysis of oxygenates over metal and metal carbide surfaces.^[41]



Scheme 3. Summary of reaction scheme and barriers. The details of atomic structures are shown in Figure S3 and S4.

3. Conclusions

In conclusion, Ti-based MXenes, viz. $\text{Ti}_3\text{C}_2\text{T}_z$ and Ti_3CNT_z , were explored as catalysts for hydrogenation of furfural using H_2 as well as 2-propanol as the hydrogen source. In the presence of H_2 , $\text{Ti}_3\text{C}_2\text{T}_z$ and Ti_3CNT_z exhibited catalytic activities of 145 and 126 $\text{mmol}_{\text{furfural}} \text{g}_{\text{catalyst}}^{-1} \text{h}^{-1}$, respectively. The activities in 2-propanol were somewhat lower at 88 and 72 $\text{mmol}_{\text{furfural}} \text{g}_{\text{catalyst}}^{-1} \text{h}^{-1}$ for $\text{Ti}_3\text{C}_2\text{T}_z$ and Ti_3CNT_z , respectively. The main product of the reaction was found to be furfuryl alcohol with a selectivity of 52% and 49% for $\text{Ti}_3\text{C}_2\text{T}_z$ and Ti_3CNT_z , respectively for reactions with H_2 and 49% and 43% for $\text{Ti}_3\text{C}_2\text{T}_z$ and Ti_3CNT_z , respectively for reaction in 2-propanol. Our results also provide evidence for oxygen removal and alcohol coupling processes using Ti-MXenes as catalysts. Stability test evidenced a better stability of Ti_3CNT_z than $\text{Ti}_3\text{C}_2\text{T}_z$ against deactivation. XRD suggested that the deactivation of $\text{Ti}_3\text{C}_2\text{T}_z$ is due to the intercalation of reaction products in MXenes. Ab initio calculations for the reaction pathways and reaction energetics on the surface of MXene indicate that metal and Bronsted

acid sites on the MXene surface can heterolytically dissociate H₂ and open up efficient proton and hydride transfer pathways that promote the selective hydrogenation as well as the hydrogenolysis of polarized C-O bonds. The acid sites on the MXene also promote acid-catalyzed etherification pathways. The hydrogen that forms on the exposed metal sites on the MXene result in high barriers for the hydrogenation the unsaturated C=C bonds and shutdown the hydrogenation of the furanic ring. These findings suggest exploring MXenes catalysts for biomass conversions.

4. Experimental and Methods Section

MAX phases synthesis. Ti₃AlC₂ was synthesized by heating a mixture of TiC (2 μm, 99.5%, Alfa Aesar) and Ti₂AlC (< 38 μm, >95%, KANTHAL), with 1:1 atomic ratio, to 1623 K with a heating rate of 10 K/min. Then, it was held at that temperature for two hours. Afterward, it was allowed to cool to room temperature (RT) in the furnace. For the synthesis of Ti₃AlCN, a mixture of Ti (< 38 μm, 99.5%, Alfa Aesar), AlN (10 μm, ≥ 98%, Sigma-Aldrich), and C (7-11 μm, 99%, Alfa Aesar), with an atomic ratio of 3:1:1, was heated to 1773 K with a rate of 10 K/min. followed by soaking at this temperature for 2 h. Then, the sample was allowed to cool to RT in the furnace. The thermal cycles for the synthesis of MAX phases were carried out in a tube furnace under a continuous flow of high purity argon. After cooling to RT, the MAX phases were ground to produce powders using titanium nitride coated stainless steel milling bit, and only powders of < 38 μm was used for synthesis of MXenes.

MXenes synthesis. Ti₃C₂T_x was synthesized at RT by immersing slowly Ti₃AlC₂ powder in an aqueous solution of hydrofluoric acid, HF (Macron Fine Chemicals – Avantor Performance Materials) with a concentration 48% HF and a ratio of 1 g Ti₃AlC₂ : 10 mL solution. The mixture was stirred for 18 h at RT using a teflon coated magnetic stir bar. After the reaction time, the mixture was centrifuged to separate the sediment from the HF solution and the solution was decanted. Then, cycles of washing using deionized (DI) water and centrifugation were repeated till the pH reached values more than 4. Afterward, the sediment was transferred from the vial to vacuum-assisted filtration device to dry the powders at RT. For Ti₃CNT_x, the same procedure as described above was used but with solution of 30% HF instead of 48%. The powders were washed and dried after the reaction as described above for the HF etching.

Catalytic tests. Furfural, F, (purity 99%, Sigma-Aldrich) hydrogenation was performed at 453 K, using a stainless steel reactor (30 mL capacity), equipped with heater, mechanical stirrer, gas supply system and thermometer. Furfural solution (15 mL; 0.3 M in 2-propanol) was added into the reactor and the desired amount of catalyst (F/catalyst ratio=50 wt/wt) was suspended

in the solution. The pressure of the hydrogen or nitrogen was 5 bar. The mixture was heated to the reaction temperature, 453K, and mechanically stirred (1250 rpm). At the end of the reaction, the autoclave was cooled down. Samples were removed periodically (0.2 mL) and HP 7820A gas chromatograph equipped with a capillary column HP-5 30m x 0.32mm, 0.25 μm Film, by Agilent Technologies. Authentic samples were analyzed to determine separation times. Quantitative analyses with external standard method (n-octanol) was used. Recycling test: Each run was carried out under the following reaction conditions: Furfural 0.3 M, and the catalyst (substrate/ catalyst = 50 wt/wt) 5 bar N_2 , 453K. The catalyst was recycled in the subsequent run after filtration without any further treatment.

Characterization. X-ray diffractions for samples investigated in this study were collected using a Cu K-alpha Scintag X1 diffractometer (Scintag, Cupertino, CA, USA). Scanning steps of 0.02° of 2θ , and 1 s dwell time at each step were used. Zeiss Merlin VP (Carl Zeiss Microscopy GmbH, Oberkochen, Germany) scanning electron microscopy (SEM) was used to investigate the changes in the morphology of the MXene particles after the reactions. X-ray photoelectron spectroscopy (XPS) data were collected using a PHI 3056 spectrometer operating an Al X-ray source operated at 15 kV and an applied power of 350 W. Samples were cold pressed between two pieces of indium, In, foil; the powder stuck to one piece of In which was mounted to the XPS stage using carbon tape. Metal leaching was checked by ICP analysis on the solution after reaction after filtration of the solid catalyst, on a JobinYvon JY24.

Theoretical calculations. All the DFT calculations reported herein were carried out using the Vienna Ab Initio Software Package (VASP)^[42] program with plane-wave basis sets and cutoff energies of 400 eV. The core electrons were treated by pseudopotentials with the projector augmented-wave (PAW) method.^[43] The Perdew–Burke–Ernzerhof (PBE) form of the gradient approximation (GGA) functional was used to model the exchange-correlation effects.^[44] Spin-polarization was employed for all calculations. The (3x3x1) unit cell of Ti_3CN MXene surface model was adapted from previous studies^[45] and was simulated with a (2x2x1) k-point mesh^[46] with a 15Å vacuum gap in the z-direction. Geometries were considered optimized when the forces on each atom were less than 0.03 eV/Å. The charge associated with each atom was subsequently calculated using the Bader analysis.^[47] The reaction pathway and activation barriers were found by the climbing image nudged elastic band (NEB) method,^[48] combined with the dimer method.^[49] The NEB band was used to find the minimal reaction path between the reactant and product states to the point where the perpendicular forces on all of the images along the band were lower than 0.1 eV/Å. The dimer method was subsequently used

to isolate the transition state to the point where the force acting on the transition state dimer was lower than 0.03 eV/ Å.

Acknowledgements

MN was partially supported as a Wigner Fellow by the Laboratory Directed Research and Development Program of Oak Ridge National Laboratory, managed by UT-Battelle, LLC, for the U.S. Department of Energy. The catalysis testing studies was supported by the Università degli Studi di Milano. XPS studies were supported by the US Department of Energy's Office of Basic Energy Sciences, Division of Materials Science and Engineering. All authors contributed to analysis of results and preparation of the manuscript. Dr Jagjit Nanda is acknowledged for the fruitful discussion.

Keywords:

Carbonitride; Furfural; Hydrogenation; MXenes; Two-dimensional

References:

- [1] a) J. N. Chheda, G. W. Huber, J. A. Dumesic, *Angew. Chem.* **2007**, *46*, 7164–7183; b) M. Besson, P. Gallezot, C. Pinel, *Chem. Rev.* **2014**, *114*, 1827–1870.
- [2] a) S. Dutta, S. De, B. Saha, M. I. Alam, *Catal. Sci. Technol.* **2012**, *2*, 2025–2036; b) S. Chen, R. Wojcieszak, F. Dumeignil, E. Marceau, S. Royer, *Chem. Rev.* **2018**, *118*, 11023–11117; c) Y. Nakagawa, M. Tamura, K. Tomishige, *ACS Catal.* **2013**, *3*, 2655–2668; d) X. Jin, B. Yin, Q. Xia, T. Fang, J. Shen, L. Kuang, C. Yang, *ChemSusChem* **2019**, *12*, 71–92.
- [3] a) S. Sitthisa, T. Sooknoi, Y. Ma, P. B. Balbuena, D. E. Resasco, *J. Catal.* **2011**, *277*, 1–13; b) D. E. Resasco, T. Sooknoi, R. G. Mallinson, S. Sitthisa, T. Pham, T. Prasomsri, *J. Catal.* **2011**, *280*, 17–27.
- [4] J. P. Lange, E. Van Der Heide, J. Van Buijtenen, R. Price, *ChemSusChem* **2012**, *5*, 150–166.
- [5] a) V. V. Pushkarev, N. Musselwhite, K. An, S. Alayoglu, G. A. Somorjai, *Nano Lett.* **2012**, *12*, 5196–5201; b) D. Liu, D. Zemlyanov, T. Wu, R. J. Lobo-Lapidus, J. A. Dumesic, J. T. Miller, C. L. Marshall, *J. Catal.* **2013**, *299*, 336–345; c) W. Zhang, Y. Zhu, S. Niu, Y. Li, *J. Mol. Catal. A: Chem.* **2011**, *335*, 71–81; d) R. Rao, A. Dandekar, R. T. K. Baker, M. A. Vannice, *J. Catal.* **1997**, *171*, 406–419; e) R. S. Rao, R. T. K.

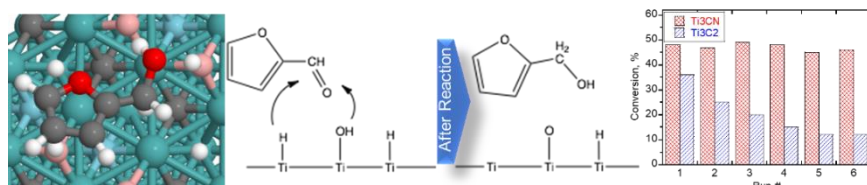
- Baker, M. A. Vannice, *Catal. Lett.* **1999**, *60*, 51–57; f) S. Campisi, C. E. Chan-Thaw, L. E. Chinchilla, A. Chutia, G. A. Botton, K. M. H. Mohammed, N. Dimitratos, P. P. Wells, A. Villa, *ACS Catal.* **2020**, *10*, 5483–5492; g) S. M. Rogers, C. R. A. Catlow, C. E. Chan-Thaw, A. Chutia, N. Jian, R. E. Palmer, M. Perdjon, A. Thetford, N. Dimitratos, A. Villa, P. P. Wells, *ACS Catal.* **2017**, *7*, 2266–2274.
- [6] Z. L. Wu, J. Wang, S. Wang, Y. X. Zhang, G. Y. Bai, L. Ricardez-Sandoval, G. C. Wang, B. Zhao, *Green Chem.* **2020**, *22*, 1432–1442.
- [7] a) J. Pang, J. Sun, M. Zheng, H. Li, Y. Wang, T. Zhang, *Appl. Catal., B* **2019**, *254*, 510–522; b) M. M. Sullivan, C. J. Chen, A. Bhan, *Catal. Sci. Technol.* **2016**, *6*, 602–616; c) K. J. Smith, *Curr. Opin. Green Sustainable Chem.* **2020**, *22*, 47–53; d) A. B. Dongil, *Nanomaterials* **2019**, *9*, 1111; e) J. A. Schaidle, L. T. Thompson, *J. Catal.* **2015**, *329*, 325–334; f) C. K. Poh, S. H. Lim, J. Lin, Y. P. Feng, *J. Phys. Chem. C* **2014**, *118*, 13525–13538; g) T. Prasomsri, M. Shetty, K. Murugappan, Y. Román-Leshkov, *Energy Environ. Sci.* **2014**, *7*, 2660–2669.
- [8] a) K. Xiong, W. S. Lee, A. Bhan, J. G. Chen, *ChemSusChem* **2014**, *7*, 2146–2149; b) W. S. Lee, Z. Wang, W. Zheng, D. G. Vlachos, A. Bhan, *Catal. Sci. Technol.* **2014**, *4*, 2340–2352; c) C. Chan-Thaw, A. Villa, *Appl. Sci.* **2018**, *8*, 259.
- [9] M. Figueras, R. A. Gutiérrez, H. Prats, F. Viñes, P. J. Ramírez, F. Illas, J. A. Rodriguez, *Phys. Chem. Chem. Phys.* **2020**, *22*, 7110–7118.
- [10] a) R. B. Levy, M. Boudart, *Science* **1973**, *181*, 547–549; b) F. H. Ribeiro, M. Boudart, R. A. Dalla Betta, E. Iglesia, *J. Catal.* **1991**, *130*, 498–513; c) E. Iglesia, J. E. Baumgartner, F. H. Ribeiro, M. Boudart, *J. Catal.* **1991**, *131*, 523–544; d) J. G. Chen, *Chem. Rev.* **1996**, *96*, 1477–1498; e) J. S. Lee, S. Locatelli, S. T. Oyama, M. Boudart, *J. Catal.* **1990**, *125*, 157–170; f) G. S. Ranhotra, A. T. Bell, J. A. Reimer, *J. Catal.* **1987**, *108*, 40–49; g) C. Liu, M. Lin, K. Fang, Y. Meng, Y. Sun, *RSC Adv.* **2014**, *4*, 20948–20954; h) H. Shou, R. J. Davis, *J. Catal.* **2013**, *306*, 91–99.
- [11] a) R. W. Gosselink, D. R. Stellwagen, J. H. Bitter, *Angew. Chem.* **2013**, *52*, 5089–5092; b) A. L. Jongerius, R. W. Gosselink, J. Dijkstra, J. H. Bitter, P. C. A. Bruijninx, B. M. Weckhuysen, *ChemCatChem* **2013**, *5*, 2964–2972; c) J. Han, J. Duan, P. Chen, H. Lou, X. Zheng, H. Hong, *ChemSusChem* **2012**, *5*, 727–733.
- [12] a) M. Naguib, V. N. Mochalin, M. W. Barsoum, Y. Gogotsi, *Adv. Mater.* **2014**, *26*, 992–1005; b) M. Naguib, M. Kurtoglu, V. Presser, J. Lu, J. Niu, M. Heon, L. Hultman, Y. Gogotsi, M. W. Barsoum, *Adv. Mater.* **2011**, *23*, 4248–4253; c) M. W. Barsoum, L. Hultman, J. Carle, J. Lu, O. Mashtalir, V. Presser, M. Naguib, Y. Gogotsi, *ACS Nano*

- 2012**, *6*, 1322–1331.
- [13] J. Halim, M. R. Lukatskaya, K. M. Cook, J. Lu, C. R. Smith, L.-Å. Näslund, S. J. May, L. Hultman, Y. Gogotsi, P. Eklund, *Chem. Mater.* **2014**, *26*, 2374–2381.
- [14] M. Naguib, R. R. Unocic, B. L. Armstrong, J. Nanda, *Dalt. Trans.* **2015**, *44*, 9353–9358.
- [15] a) D. Er, J. Li, M. Naguib, Y. Gogotsi, V. B. Shenoy, *ACS Appl. Mater. Interfaces* **2014**, *6*, 11173–11179; b) M. Naguib, B. Dyatkin, V. Presser, M. W. Barsoum, P. Simon, Y. Gogotsi, J. Come, P.-L. Taberna, *Electrochem. commun.* **2012**, *16*, 61–64; c) M. Naguib, J. Halim, J. Lu, K. M. Cook, L. Hultman, Y. Gogotsi, M. W. Barsoum, *J. Am. Chem. Soc.* **2013**, *135*, 15966–15969; d) M. Naguib, M. W. Barsoum, Y. Dall’Agnese, H. L. Zhuang, Y. Gogotsi, P. R. C. Kent, Y. Xie, *ACS Nano* **2014**, *8*, 9606–9615; e) M. R. Lukatskaya, Y. Dall’Agnese, M. Naguib, M. W. Barsoum, C. E. Ren, O. Mashtalir, P. Simon, P. L. Taberna, Y. Gogotsi, P. Rozier, *Science* **2013**, *341*, 1502–1505; f) M. Ghidui, M. R. Lukatskaya, M. Q. Zhao, Y. Gogotsi, M. W. Barsoum, *Nature* **2015**, *516*, 78–81; g) Y. Dall’Agnese, P. L. Taberna, Y. Gogotsi, P. Simon, *J. Phys. Chem. Lett.* **2015**, *6*, 2305–2309; h) X. Wang, S. Kajiyama, H. Iinuma, E. Hosono, S. Oro, I. Moriguchi, M. Okubo, A. Yamada, *Nat. Commun.* **2015**, *6*, 6544; i) M. Naguib, R. A. Adams, Y. Zhao, D. Zemlyanov, A. Varma, J. Nanda, V. G. Pol, *Chem. Commun.* **2017**, *53*, 6883–6886.
- [16] a) Q. Peng, J. Guo, Q. Zhang, J. Xiang, B. Liu, A. Zhou, R. Liu, Y. Tian, *J. Am. Chem. Soc.* **2014**, *136*, 4113–4116; b) Y. Ying, Y. Liu, X. Wang, Y. Mao, W. Cao, P. Hu, X. Peng, *ACS Appl. Mater. Interfaces* **2015**, *7*, 1795–1803; c) C. E. Ren, K. B. Hatzell, M. Alhabeb, Z. Ling, K. A. Mahmoud, Y. Gogotsi, *J. Phys. Chem. Lett.* **2015**, *6*, 4026–4031; d) Q. Zhang, J. Teng, G. Zou, Q. Peng, Q. Du, T. Jiao, J. Xiang, *Nanoscale* **2016**, *8*, 7085–7093.
- [17] a) H. Liu, C. Duan, C. Yang, W. Shen, F. Wang, Z. Zhu, *Sens. Actuators, B* **2015**, *218*, 60–66; b) B. Xu, M. Zhu, W. Zhang, X. Zhen, Z. Pei, Q. Xue, C. Zhi, P. Shi, *Adv. Mater.* **2016**, *28*, 3333–3339; c) D. Xiao, Y. Tang, C. Yang, J. Zhu, F. Wang, C. Duan, *J. Electrochem. Soc.* **2014**, *162*, B16–B21; d) J. Chen, K. Chen, D. Tong, Y. Huang, J. Zhang, J. Xue, Q. Huang, T. Chen, *Chem. Commun.* **2015**, *51*, 314–317; e) E. S. Muckley, M. Naguib, H. W. Wang, L. Vlcek, N. C. Osti, R. L. Sacci, X. Sang, R. R. Unocic, Y. Xie, M. Tyagi, E. Mamontov, K. L. Page, P. R. C. Kent, J. Nanda, I. N. Ivanov, *ACS Nano* **2017**, *11*, 11118–11126.
- [18] X. Xie, S. Chen, W. Ding, Y. Nie, Z. Wei, *Chem. Commun.* **2013**, *49*, 10112–10114.

- [19] X. Li, G. Fan, C. Zeng, *Int. J. Hydrogen Energy* **2014**, *39*, 14927–14934.
- [20] X. Li, C. Zeng, G. Fan, *Int. J. Hydrogen Energy* **2015**, *40*, 9217–9224.
- [21] X. Li, C. Zeng, G. Fan, *Int. J. Hydrogen Energy* **2015**, *40*, 3883–3891.
- [22] Y. Gao, L. Wang, Z. Li, A. Zhou, Q. Hu, X. Cao, *Solid State Sci.* **2014**, *35*, 62–65.
- [23] a) T. Su, R. Peng, Z. D. Hood, M. Naguib, I. N. Ivanov, J. K. Keum, Z. Qin, Z. Guo, Z. Wu, *ChemSusChem* **2018**, *11*, 688–699; b) Z. D. Hood, H. Wang, Z. Wu, M. Naguib, R. Peng, S. P. Adhikari, *ChemSusChem* **2016**, *9*, 1490–1497.
- [24] Y. Liu, H. Du, X. Zhang, Y. Yang, M. Gao, H. Pan, *Chem. Commun.* **2016**, *52*, 705–708.
- [25] T. Y. Ma, J. L. Cao, M. Jaroniec, S. Z. Qiao, *Angew. Chem.* **2016**, *55*, 1138–1142.
- [26] G. Gao, A. P. O’Mullane, A. Du, *ACS Catal.* **2017**, *7*, 494–500.
- [27] a) J. He, L. Schill, S. Yang, A. Riisager, *ACS Sustainable Chem. Eng.* **2018**, *6*, 17220–17229; b) T. Yang, H. Li, J. He, Y. Liu, W. Zhao, Z. Wang, X. Ji, S. Yang, *ACS Omega* **2017**, *2*, 1047–1054.
- [28] J. Diao, M. Hu, Z. Lian, Z. Li, H. Zhang, F. Huang, B. Li, X. Wang, D. S. Su, H. Liu, *ACS Catal.* **2018**, *8*, 10051–10057.
- [29] E. Blanco, A. Rosenkranz, R. Espinoza-González, V. M. Fuenzalida, Z. Zhang, S. Suárez, N. Escalona, *Catal. Commun.* **2020**, *133*, 105833.
- [30] S. Hamelet, T. Tzedakis, J.-B. Leriche, S. Sailler, D. Larcher, P.-L. Taberna, P. Simon, J.-M. Tarascon, *J. Electrochem. Soc.* **2012**, *159*, A1360–A1367.
- [31] S. Kajiyama, L. Szabova, K. Sodeyama, H. Iinuma, R. Morita, K. Gotoh, Y. Tateyama, M. Okubo, A. Yamada, *ACS Nano* **2016**, *10*, 3334–3341.
- [32] I. R. Shein, A. L. Ivanovskii, *Comput. Mater. Sci.* **2012**, *65*, 104–114.
- [33] W. Sun, H. W. Wang, L. Vlcek, J. Peng, A. B. Brady, N. C. Osti, E. Mamontov, M. Tyagi, J. Nanda, S. G. Greenbaum, P. R. C. Kent, M. Naguib, *Adv. Mater. Interfaces* **2020**, *7*, 1902207.
- [34] I. Shilov, A. Smirnov, O. Bulavchenko, V. Yakovlev, I. N. Shilov, A. A. Smirnov, O. A. Bulavchenko, V. A. Yakovlev, *Catalysts* **2018**, *8*, 560.
- [35] Y. Deng, R. Gao, L. Lin, T. Liu, X.-D. Wen, S. Wang, D. Ma, *J. Am. Chem. Soc.* **2018**, *140*, 14481–14489.
- [36] P. Jia, X. Lan, X. Li, T. Wang, *ACS Sustainable Chem. Eng.* **2018**, *6*, 13287–13295.
- [37] H. Chen, H. Ruan, X. Lu, J. Fu, T. Langrish, X. Lu, *Mol. Catal.* **2018**, *445*, 94–101.
- [38] J. He, S. Yang, A. Riisager, *Catal. Sci. Technol.* **2018**, *8*, 790–797.
- [39] F. Wang, Z. Zhang, *ACS Sustainable Chem. Eng.* **2017**, *5*, 942–947.

- [40] J. Macht, M. J. Janik, M. Neurock, E. Iglesia, *J. Am. Chem. Soc.* **2008**, *130*, 10369–10379.
- [41] a) M. M. Sullivan, J. T. Held, A. Bhan, *J. Catal.* **2015**, *326*, 82–91; b) M. Chia, Y. J. Pagán-Torres, D. Hibbitts, Q. Tan, H. N. Pham, A. K. Datye, M. Neurock, R. J. Davis, J. A. Dumesic, *J. Am. Chem. Soc.* **2011**, *133*, 12675–12689.
- [42] G. Kresse, *Phys. Rev. B* **2000**, *62*, 8295–8305.
- [43] a) G. Kresse, D. Joubert, *Phys. Rev. B* **1999**, *59*, 1758–1775; b) P. E. Blöchl, *Phys. Rev. B* **1994**, *50*, 17953–17979.
- [44] J. P. Perdew, K. Burke, M. Ernzerhof, *Phys. Rev. Lett.* **1996**, *77*, 3865–3868.
- [45] Y. Xie, M. Naguib, V. N. Mochalin, M. W. Barsoum, Y. Gogotsi, X. Yu, K. W. Nam, X. Q. Yang, A. I. Kolesnikov, P. R. C. Kent, *J. Am. Chem. Soc.* **2014**, *136*, 6385–6394.
- [46] H. J. Monkhorst, J. D. Pack, *Phys. Rev. B* **1976**, *13*, 5188–5192.
- [47] W. Tang, E. Sanville, G. Henkelman, *J. Phys.: Condens. Matter* **2009**, *21*, 084204.
- [48] a) G. Henkelman, B. P. Uberuaga, H. Jónsson, *J. Chem. Phys.* **2000**, *113*, 9901–9904; b) G. Henkelman, H. Jónsson, *J. Chem. Phys.* **2000**, *113*, 9978–9985.
- [49] G. Henkelman, H. Jónsson, *J. Chem. Phys.* **1999**, *111*, 7010–7022.

Table of Contents:



Both titanium carbides and carbonitrides MXenes catalyzed the conversion of furfural into furfural alcohol by hydrogenation with catalytic activities of 145 and 126 $\text{mmol}_{\text{furfural}} \text{g}_{\text{catalyst}}^{-1} \text{h}^{-1}$, respectively. The carbonitride showed better catalytic stability combined with no swelling in the *d*-spacing compared to their carbide counterparts. Ab initio calculations were used to explore the reaction pathway on the surface of MXene. The findings of this study suggest exploring MXenes catalysts for biomass conversions.